Missouri University of Science and Technology
Scholars' Mine

Economics Faculty Research & Creative Works | Economics

01 Jul 2004

Artificial Neural Network Modeling of RF MEMS Resonators

Yongjae Lee

Yonghwa Park

Feng Niu

Bonnie Bachman
Missouri University of Science and Technology, bachmanb@mst.edu

et. al. For a complete list of authors, see https://scholarsmine.mst.edu/econ_facwork/124

Follow this and additional works at: https://scholarsmine.mst.edu/econ_facwork

Part of the Materials Science and Engineering Commons

Recommended Citation

Lee, Y., Park, Y., Niu, F., Bachman, B., Gupta, K. C., & Filipovic, D. (2004). Artificial Neural Network Modeling of RF MEMS Resonators. *International Journal of RF and Microwave Computer-Aided Engineering, 14*(4), pp. 302-316. Wiley.
The definitive version is available at https://doi.org/10.1002/mmce.20017

This Article - Journal is brought to you for free and open access by Scholars' Mine. It has been accepted for inclusion in Economics Faculty Research & Creative Works by an authorized administrator of Scholars' Mine. This work is protected by U. S. Copyright Law. Unauthorized use including reproduction for redistribution requires the permission of the copyright holder. For more information, please contact scholarsmine@mst.edu.

Artificial Neural Network Modeling of RF MEMS Resonators

Yongjae Lee,[1] Yonghwa Park,[1] Feng Niu,[2] Bonnie Bachman,[3] K.C. Gupta,[1] Dejan Filipovic[1]

[1] Center for Advanced Manufacturing and Packaging of Microwave, Optical, and Digital Electronics (CAMPmode) and Department of Electrical and Computer Engineering, University of Colorado at Boulder, Boulder, CO 80309
[2] Motorola, Inc., Florida Communication Research Labs, Plantation, FL 33322
[3] Motorola, Inc., IDEN-WLAN Technology, Plantation, FL 33322

Received 2 September 2003; accepted 23 January 2004

ABSTRACT: In this article, a novel and efficient approach for modeling radio-frequency microelectromechanical system (RF MEMS) resonators by using artificial neural network (ANN) modeling is presented. In the proposed methodology, the relationship between physical-input parameters and corresponding electrical-output parameters is obtained by combined circuit/full-wave/ANN modeling. More specifically, in order to predict the electrical responses from a resonator, an analytical representation of the electrical equivalent-network model (EENM) is developed from the well-known electromechanical analogs. Then, the reduced-order, nonlinear, dynamic macromodels from 3D finite-element method (FEM) simulations are generated to provide training, validating, and testing datasets for the ANN model. The developed ANN model provides an accurate prediction of an electrical response for various sets of driving parameters and it is suitable for integration with an RF/microwave circuit simulator. Although the proposed approach is demonstrated on a clamped-clamped (C-C) beam resonator, it can be readily adapted for the analysis of other micromechanical resonators. © 2004 Wiley Periodicals, Inc. Int J RF and Microwave CAE 14: 302–316, 2004.

Keywords: artificial neural networks; computer-aided design; equivalent circuits; finite-element methods; microelectromechanical devices

I. INTRODUCTION

Several full-wave numerical methods, including boundary element (BE), finite element (FE), and finite-difference time-domain (FDTD) [1–4], are currently being used for an accurate modeling of RF MEMS devices. Although these methods provide necessary accuracy, they are generally limited to a single analysis for a specific structure, and their computational overhead (running time, memory) becomes extensive when a number of simulations with different mesh properties are needed. On the other hand, ANN-based algorithms have a great advantage in reducing the computational cost, especially when implemented within a circuit simulator that has integrated fine-tuning and optimization options. Based on the massively parallel nature of a neural network model, which is capable of modeling nonlinear mappings of multiple input/output variables, this approach has provided an accurate device characterization and efficient

Correspondence to: Dejan Filipovic; email: dejan@Colorado.edu.

Published online in Wiley InterScience (www.interscience.wiley.com). DOI 10.1002/mmce.20017

© 2004 Wiley Periodicals, Inc.

prediction of unknown input-output relationships with low computational overhead. Thus, it allows fast calculation of output values for a set of arbitrary input parameters. The main disadvantage of ANN modeling is the extensive time and effort needed to prepare the training dataset, which sometimes can be too difficult to obtain.

Due to their electrical and mechanical nature, MEMS devices traditionally have been analyzed in both electrical and mechanical domains [5–7]. Coupling between the two domains was achieved using empirical/analytical expressions or via full-wave analysis. An alternative way of analyzing MEMS devices (RF MEMS resonator in our case) is to employ ANN modeling. To do so, several classical approaches for the modeling of electromechanical devices and systems must be utilized. It is necessary, for example, to develop a macromodel for the resonator's mechanical behavior. Then, a full-wave method must be used to capture all essential characteristics, including nonlinearities and parasitic effects of the MEMS resonator. From this analysis, a set of physical parameters, such as the damping coefficient, stiffness, and effective mass of the resonator, can be extracted. The obtained parameters can be inserted into the EENM to produce the electrical/dynamic responses using electromechanical analogs [8]. The EENM provides a convenient method for modeling and simulating the behavior characteristics of a RF MEMS resonator, since electrical/dynamic outputs are obtained without utilizing thousands of degrees of freedom (DOF), as in the case of a full-wave FEM simulation.

In this article, an ANN-based modeling approach is proposed for the efficient analysis of the C-C beam RF MEMS resonator. The model is trained by appropriately selected datasets from both the FEM simulator [9] and EENM, and it is constructed by the use of the neural network design (NND) toolbox in MATLAB [10]. A methodology is demonstrated in which a feed-forward (FF) back-propagation network is implemented to model the selected resonator. The inputs to the ANN model are the geometrical parameters of the resonator (length, width, DC-bias voltage, and resonator-to-electrode gap), while the outputs are resonant frequency, dynamic and static output currents, input impedance, and beam displacement. Once the ANN model is generated, its implementation in an RF/microwave circuit simulator makes a fast prediction of electrical-circuit responses for a wide range of geometrical parameters and excitations feasible. A similar procedure can be applied to MEMS-based circuits and devices such as switches, accelerometers, micromirrors, and so forth. For example, the performance of a CPW-based MEMS capacitive switch is dependent on the geometrical variations of the switch, such as bridge dimensions, air gap, CPW gap, and so on. [11, 12]. Provided that an adequate training dataset is obtained from either measurements or a full-wave simulation, the ANN should successfully approximate the desired input/output mapping within the ranges of the valid device parameters.

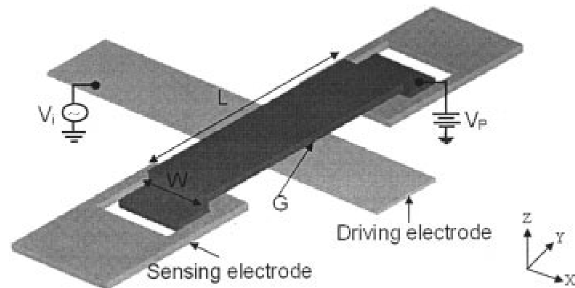

Figure 1. Configuration of a C-C beam RF MEMS resonator.

This article is organized as follows. In section II, the C-C beam resonating structure is introduced. A methodology for building an ANN model is discussed and demonstrated in sections III and IV. The results are presented in section V. A review of the electromechanical analogs and the derivation of the EENM are given in the Appendix.

II. CLAMPED-CLAMPED BEAM RF MEMS RESONATOR

The C-C beam RF MEMS resonator [13] is selected as the device for which an ANN model will be derived. It is important to note that a similar methodology can be applied to other structures, such as free-free beam and circular-disk resonators [13, 14]. The schematic of a C-C beam resonator is shown in Figure 1. The appropriate geometrical parameters and material properties, as well as DC-bias voltage and AC excitation, are given in Table I.

The resonator is composed of a fixed beam suspended over an underlying electrode [15]. The superposition of DC-bias and AC-signal voltages induces the electrostatic force and time-varying force, thus generating the vibration of the resonating beam in the vertical *z*-direction. The zero-to-peak displacement amplitude at the center of the beam is obtained when the frequency of the AC excitation source matches the natural frequency, which is determined by the physical parameters of the structure. Deterministic static capacitance per unit dis-

TABLE I. Parameters of a C-C Beam RF MEMS Resonator

Parameter	Value	Unit
Resonator-beam length	16	μm
Resonator-beam width	8	μm
Resonator-beam thickness	2.1	μm
Electrode area	8×8	μm^2
Electrode-to-resonator gap	0.07	μm
Anchor area	$8 \times 8 \times 2$	μm^2
Elastic modulus of polysilicon	150	GPa
Density of polysilicon	2300	kg/m^3
Poisson's ratio	0.29	—
DC-bias voltage	35	V
Magnitude of AC-signal voltage	2	mV

placement is computed at the center of the resonating beam when the beam is vibrating at the natural frequency. The change of resonator-to-electrode capacitance per unit displacement induces a time-varying current, which can be measured at the sensing electrode under the resonating beam. By changing the geometrical parameters (such as the resonating-beam length and width, the gap between the resonating beam and the electrode, and the DC-bias voltage), the corresponding electrical responses can be obtained. The methodology used to realize the characterization of these electrical responses (resonant frequency, input impedance, output current, and so forth), is demonstrated in the following sections.

The first few mode shapes of the C-C beam resonator are given in Figure 2. As expected, the wave propagation prevails along the length of the resonator (the y-direction in Fig. 1). When the frequency of an AC excitation matches the fundamental frequency of the resonator, the wavelength associated with the first mode is comparable to the length of the resonator. In addition, the maximum displacement of the resonating beam and the largest output current are observed for the first mode. Therefore, this mode is the most dominant and will be used to develop a lumped-parameter model.

The C-C beam RF MEMS resonator that operates near the natural frequency can be modeled by a parallel RLC circuit, which represents the dynamic components of the vibrations. The dynamic components are related to the mass, stiffness, and damping coefficient of the beam. Electromechanical analogies are used to convert a mechanical system into its electrical analog, which thus allows the analysis of an equivalent model in the electrical domain [16, 17]. The analogies and derivation of the EENM are given in the Appendix.

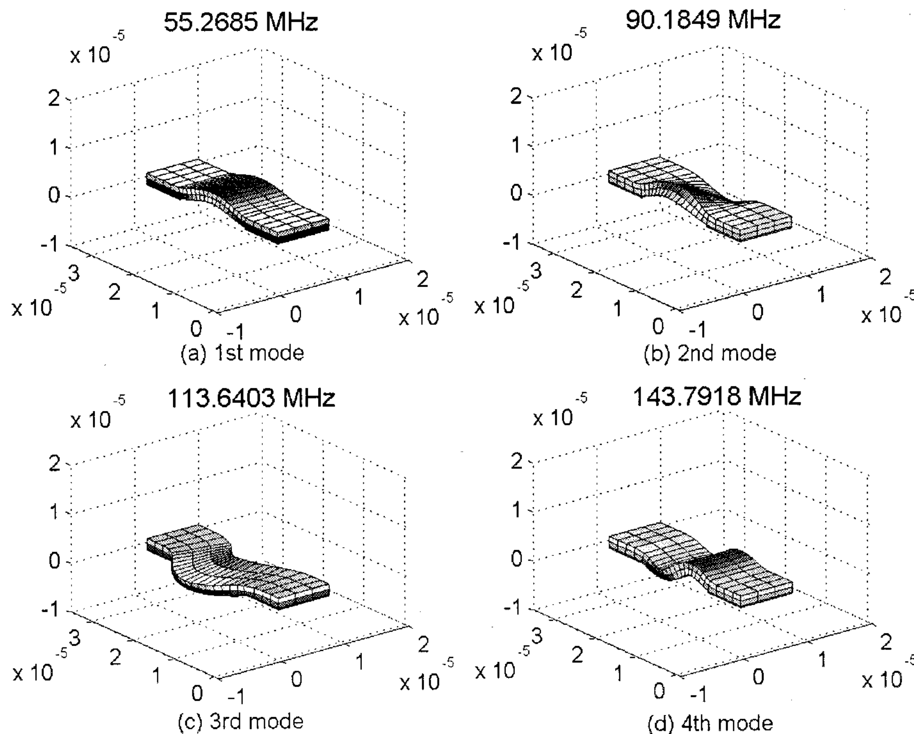

Figure 2. First four electromechanical mode shapes of a C-C beam resonator based on the geometrical parameters in Table I.

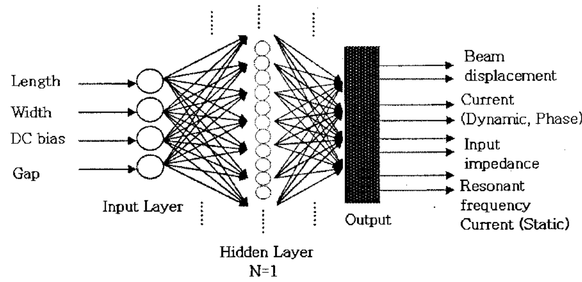

Figure 3. Architecture of a two-layer ANN with the set of input-output pair parameters.

III. ANN MODELING

The ANN architecture that will be used to obtain the electrical responses is shown in Figure 3. It consists of one input layer and one hidden layer with 36 neurons. The strength of the connections between neurons is described by the coefficients comprising a weight vector. Learning is accomplished by adjusting these coefficients until the network provides output results with prescribed values.

To begin, a Levenberg–Marquardt (LM) backpropagation algorithm [18] is used for training, and the number of neurons and hidden layers are chosen based on observations from Figure 4. A distinctive improvement of the mean square error (MSE) is seen as the number of neurons increases. It is seen that a local minimum MSE better than 1.67E-04 is reached with 30 to 40 neurons for both one and two-hidden-layers. Note that there is an increase of MSE after passing through the first local minimum, which implies that the ANN starts overfitting at that point In order to avoid this overfitting, 36 hidden neurons with one hidden layer are selected. As expected, the convergence time is much shorter for the one hidden layer [see Fig. 4(b)].

Input vectors for the ANN model are the geometrical parameters of the C-C beam resonator. The range of input variables is determined by the desired model-usage requirements (see Table II). Among the input parameters, the electrode width is assumed to be the same as the resonating beam width and the magnitude of the input AC signal source is 2 mV (as used throughout this article). In order to train the ANN model, a number of simulations need to be performed using a full-wave simulator (FEM in our case). In the input-parameter dataset, some combinations of DC-bias voltages and geometrical parameters (resonator width and length) result in the resonating beam collapsing down to the electrode. To avoid unreasonable datasets, dataset verification is executed through the graphical investigation of each resonant-mode shape. This procedure led to the removal of about 5% of the datasets from the electrical network model. In addition, training, validating, and testing datasets are carefully generated, so that they are different from each other.

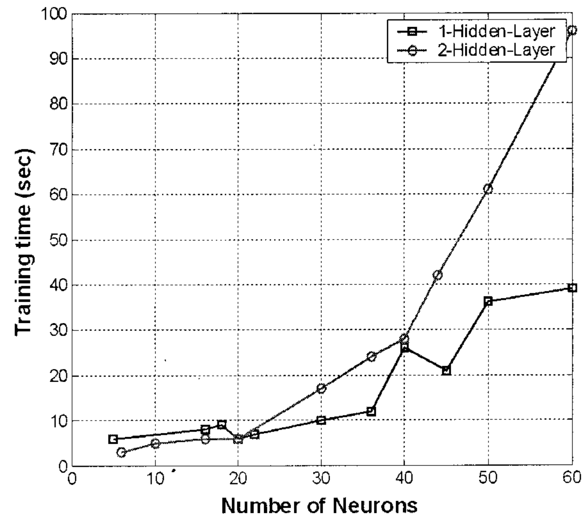

(a)

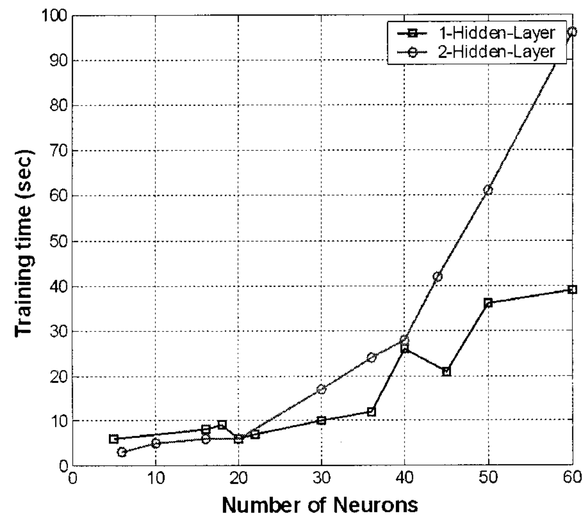

(b)

Figure 4. (a) MSE vs. the number of neurons in the hidden layer and (b) number of neurons vs. the elapsed time to reach MSE.

TABLE II. Selection of the Range of Input Variables for the ANN Model

Input Parameters	Range	No. of Steps
Resonator length [μm]	10–30	8
Resonator width [μm]	6–24	10
Gap [μm]	0.05–0.2	8
DC-bias voltage [V]	20–200	8

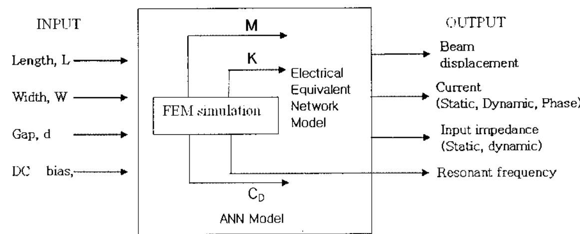

Figure 5. Block diagram of the ANN model.

IV. PREPARATION OF THE TRAINING DATA FOR THE ANN MODEL

An ANN training dataset for the C-C beam RF MEMS resonator is prepared from both the FEM simulator and EENM. Once the results from the FEM simulator are validated, data generation by the simulator has a number of advantages compared to that by experiment. Any input parameter can be changed easily, because it is only a numerical change and does not involve any physical/experimental change. Output data from the simulator are the effective mass of the resonating beam M, stiffness K, damping coefficient C_D, and resonant frequency, as shown in Figure 5. Note that once the ANN model is developed, there is no need to execute a tedious and time-consuming two-stage simulation process for obtaining various electrical responses.

The range of input and output parameters obtained from the FEM simulator and the EENM is given in Table III. Due to the given material properties (see Table I) and the limitation in achievable resonant frequency for the case of a C-C beam-resonating structure [19], the input-output pair ranges are determined as shown in Table III. The ANN model has been developed for the C-C beam RF MEMS resonator in the 11–120-MHz range of resonant frequencies.

V. RESULTS

The Levenberg–Marquardt (LM) and conjugate-gradient (CG) algorithms are compared in order to obtain the ANN model for the C-C beam RF MEMS resonator. A two-layer feed-forward back-propagation network is created with a four-element input and LOGSIG neurons in the hidden layer. The ANN model, trained with 210 training datasets, converged with MSE values of 1.38E-4 and 5.70E-3 using the LM and CG algorithms, respectively. The MSE has been chosen as a performance index for each training method, as shown in Figure 6. The MSE for the validating dataset is monitored during the training process in order to avoid overfitting of the training dataset by performing simultaneous training and testing of ANN (see Fig. 6). When the network begins to overfit the training data, the error on the validating dataset will typically begin to increase, thus resulting in the termination of the training process. In the case of the LM method, it took 16 iterations and 10 sec on a PC (Pentium 4, CPU 1.9 GHz) to meet the desired MSE. The CG algorithm stopped after 62 iterations, but did not reach the desired goal. Instead, it converged to the MSE of $\sim 10^{-3}$. It was found that although the LM method requires more stringent computational capabilities, it is a significantly faster and preferable method to the CG algorithm.

By comparing the ANN models utilizing the LM (Fig. 7) and CG (Fig. 8) algorithms, it was observed that the trained data are dispersed with the insufficient correlations using the CG method. This means that the required MSE from a CG algorithm should be reduced to less than an order of 10^{-3}. In order to prepare a well-trained ANN model, the LM method is preferred to that of the CG in this case. The LM algorithm appears to be the faster ANN training algorithm, ir-

TABLE III. Input and Output Parameters and Their Ranges for Training the ANN Model

Input Parameters	Range	No. of Steps	Output Parameters	Range
Resonator length L [μm]	10–30	8	Static beam displacement at DC [nm]	0.11–20
			Dynamic beam displacement at AC [nm]	0.003–5.2
Resonator width W [μm]	6–24	10	Static input impedance [MΩ]	0.1–6 K
			Dynamic input impedance [MΩ]	0.8–13 K
Gap d [μm]	0.05–0.2	8	Static output current [mA]	0.009–127
			Dynamic output current [μA]	0.009–16
DC-bias voltage V [V]	20–200	8	Phase of dynamic output current [deg]	23–37
			Resonant frequency [MHz]	11–120

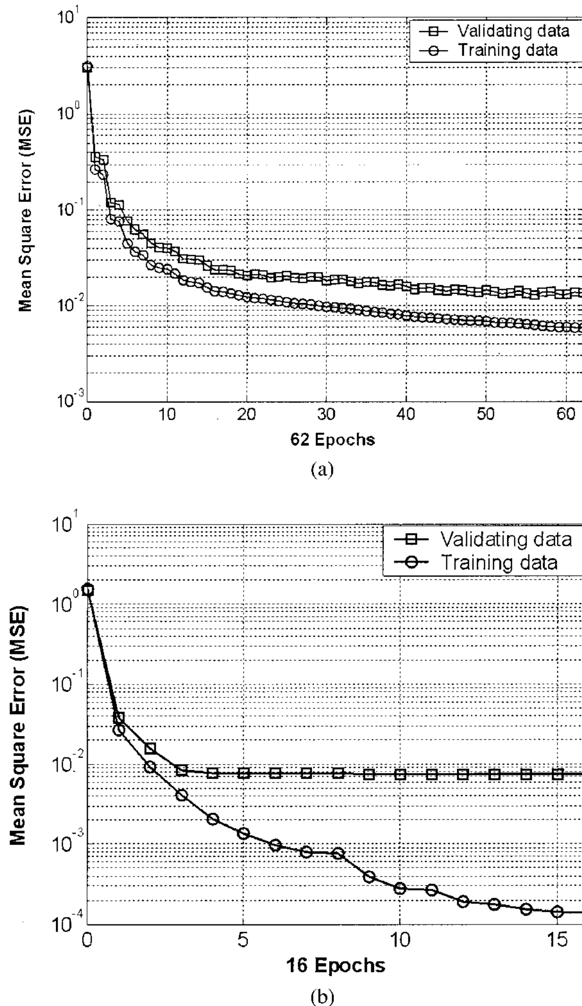

Figure 6. Comparison of MSE after training the ANN model using the (a) conjugate-gradient and (b) Levenberg–Marquardt training algorithms.

respective of the large number of computations [20]. Once the ANN model is trained, it needs to be tested using the testing dataset, which is not used in any capacity for training the ANN. Upon inserting the testing dataset into the developed ANN model, the excellent correlation between the ANN model and the testing dataset is observed for all resonator parameters (see Fig. 9).

After training, the relationships between the geometrical inputs and various outputs are obtained (see Fig. 10). It is seen that good agreement between the ANN model and the simulated data (EENM) is obtained with the relative error between 0.9% and 3%. As the resonating beam length is increased, the resonant frequency is decreased [see Fig. 10(a)]. On the other hand, the resonant frequency is slightly increased with the increase of the beam width [see Fig. 10(b)]. The dynamic output current is affected by a displacement between the resonating beam and the electrode, that is, as the gap across two beams increases, the dynamic output current rapidly decreases [see Fig. 10(c)]. Note that the maximum displacement (in the vertical direction) of the beam occurs when it vibrates in the first mode shape for the lumped-parameters case (see Fig. 2). Physically, the first mode shape has a vertically symmetrical deformation, so that the dominant wave propagates in the direction along the length of the resonating beam. Thus, the maximum dynamic-output current is induced for the fundamental mode of the resonating beam, as shown in Figure 11.

For further validation of the proposed method, the resonant frequency, insertion loss, and dynamic output current are extracted and compared with the relevant model from the ADS [21]. As depicted in Figure 11, excellent agreement between the ANN and EENM models is obtained. Note that the electrical stiffness K_E [$\sim V^2/d_0^3$, see eq. (A11)] was also considered in computing the resonant frequency. The device responses for the three models are compared (see Table IV) and their dynamic current responses are computed in the frequency domain. It is seen that the maximum dynamic-output current is induced at the center frequency for each case [see Fig. 12 (a)]. Figures 12(b) and 12(c) illustrate the dynamic-output current response of the beam in the time domain (L = 16μm, W = 7μm, gap = 0.08μm) when actuated by a DC bias (30 V) and AC sinusoidal excitations (amplitude = 2 mV; frequency $\sim$ 53 MHz). To demonstrate the low computational cost of the proposed methodology, the computational times for the FEM model, the ANN model, and the model in ADS are shown in Table VI. It is clear that a large savings in the CPU time is obtained by using the ANN model. Note that the simulation time of the integrated ANN model is similar to that of the ANN model before integration.

VI. CONCLUSION

An accurate and efficient ANN-based approach for modeling C-C beam RF MEMS resonators has been developed. The electrical responses of a C-C beam RF MEMS resonator are obtained through combined full-wave/circuit/ANN modeling. The developed model is integrated within the ADS circuit simulator, thus allowing system-level circuit analysis and design, as well as device and/or circuit tuning and optimization. The developed methodology contributes to the re-

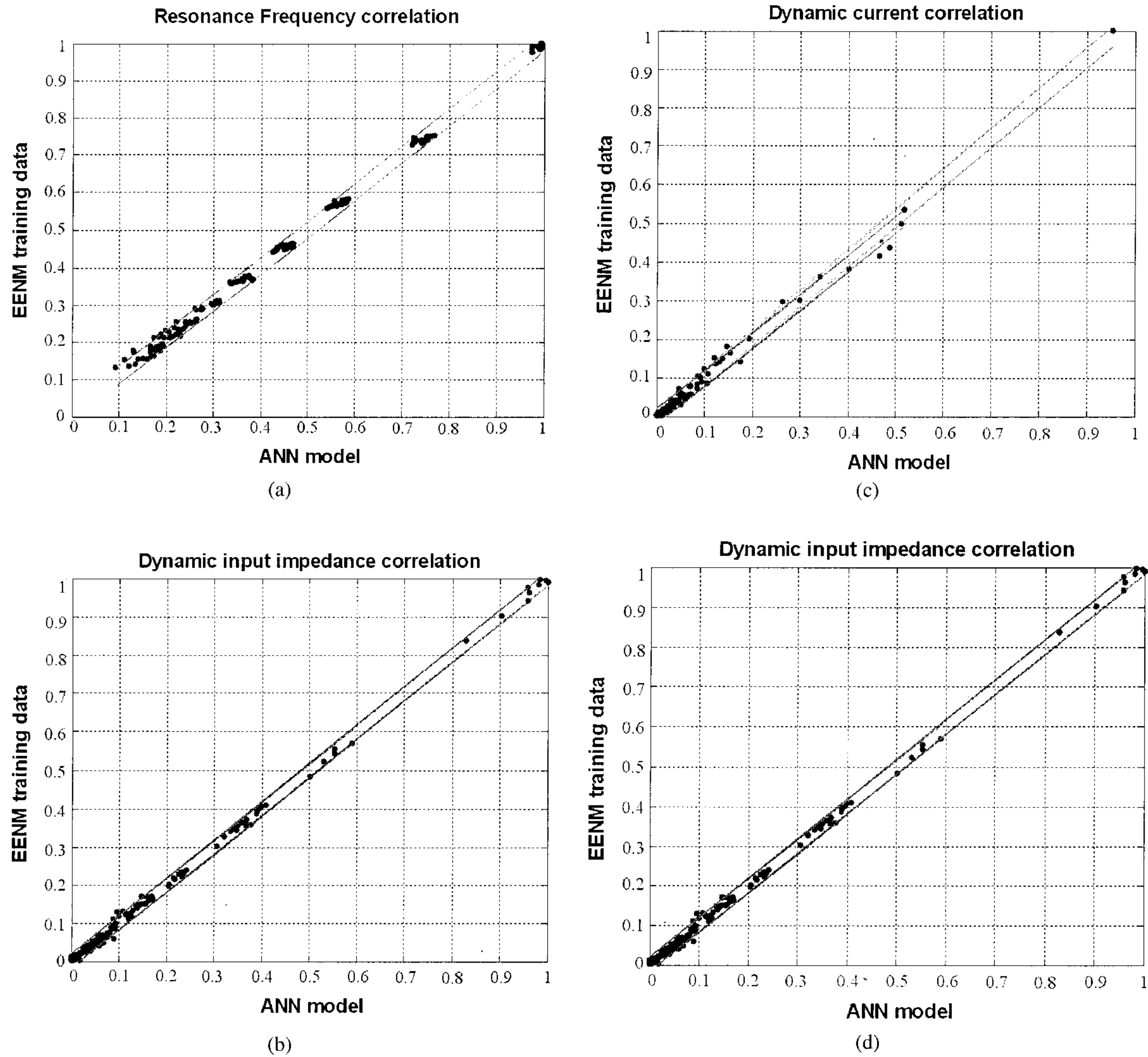

Figure 7. Comparison of the ANN-model results with the electrical-network model of the C-C beam resonator for the training dataset using the LM training algorithm: (a) resonant-frequency response with 0.9986 correlation coefficient; (b) magnitude of dynamic-input impedance response with 0.9917 correlation coefficient; (c) magnitude of dynamic-current response with 0.9912 correlation coefficient; (d) amplitude of dynamic beam-displacement response with 0.9751 correlation coefficient at AC-signal voltage.

duced simulation time, effort, and associated cost while preserving the accuracy of the full-wave model. The development of the ANN model for other RF MEMS resonating structures and the corresponding accurate representation of an electrical equivalent network model (EENM) describing a distributed-parameter system are topics of future work.

ACKNOWLEDGMENT

The authors are grateful to the Motorola, Inc. for support of this project and also thank CAMP mode, a National Science Foundation Industry/University Cooperative Research Center.

APPENDIX: DERIVATION OF EQUATIONS FOR THE ELECTRICAL EQUIVALENT NETWORK MODEL

The appropriate mechanical and electrical-circuit models for the structure of a C-C beam resonator are shown in Figures 13(a) and 13(b), respectively. From Figure 13(a), we can write the motion equation as

$$F = M\frac{d^2z}{dt^2} + C_D\frac{dz}{dt} + Kz,$$

$$\text{where } \frac{dz}{dt} = v(\text{velocity}), \quad \text{(A1)}$$

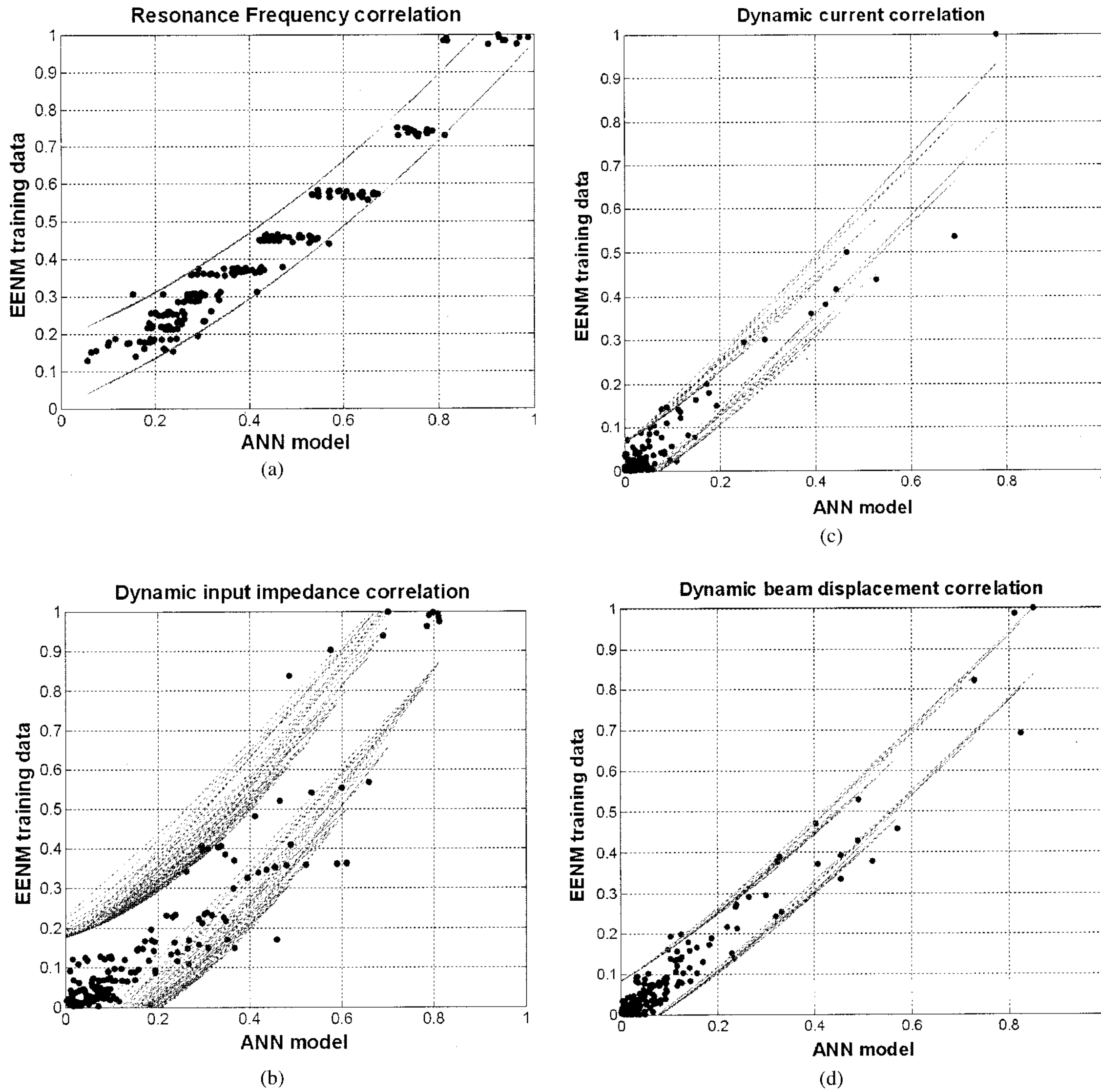

Figure 8. Comparison of the ANN-model results with the electrical-network model of the C-C beam resonator for the training dataset using the CG training algorithm: (a) resonant-frequency response with 0.9733 correlation coefficient; (b) magnitude of dynamic-input impedance response with 0.9913 correlation coefficient; (c) magnitude of dynamic-current response with 0.9533 correlation coefficient; (d) amplitude of dynamic beam-displacement response with 0.9733 correlation coefficient.

while the circuit equation of Figure 13(b) can be formulated as

$$\frac{1}{L} I_F = C \frac{d^2 i_L}{dt^2} + \frac{1}{R} \frac{di_L}{dt} + \frac{1}{L} i_L = \frac{1}{L} (i_C + i_R + i_L). \tag{A2}$$

In (A2), i_L denotes the current through the inductance and I_F is a current source analogous to the force applied across the resonator. Relevant analogies between the corresponding mechanical and electrical parameters are obtained by a direct comparison between eqs. (A1) and (A2), as shown in Table V. These will be used for the electrical characterization of the C-C beam RF MEMS resonator.

The capacitance C(t) across the beams is given by:

$$C(t) = \frac{\varepsilon_0 A}{d_0 - (z_0 + \mathrm{Re}\{\bar{z}_i e^{j\omega t}\})} \tag{A3}$$

where A is the overlapped surface area between the two beams ($W_e W_r$). When both a DC-bias voltage and an AC-signal source $((v_i(t) = \bar{V}_i e^{j\omega t}, \bar{V}_i = V_i e^{j\varphi}))$

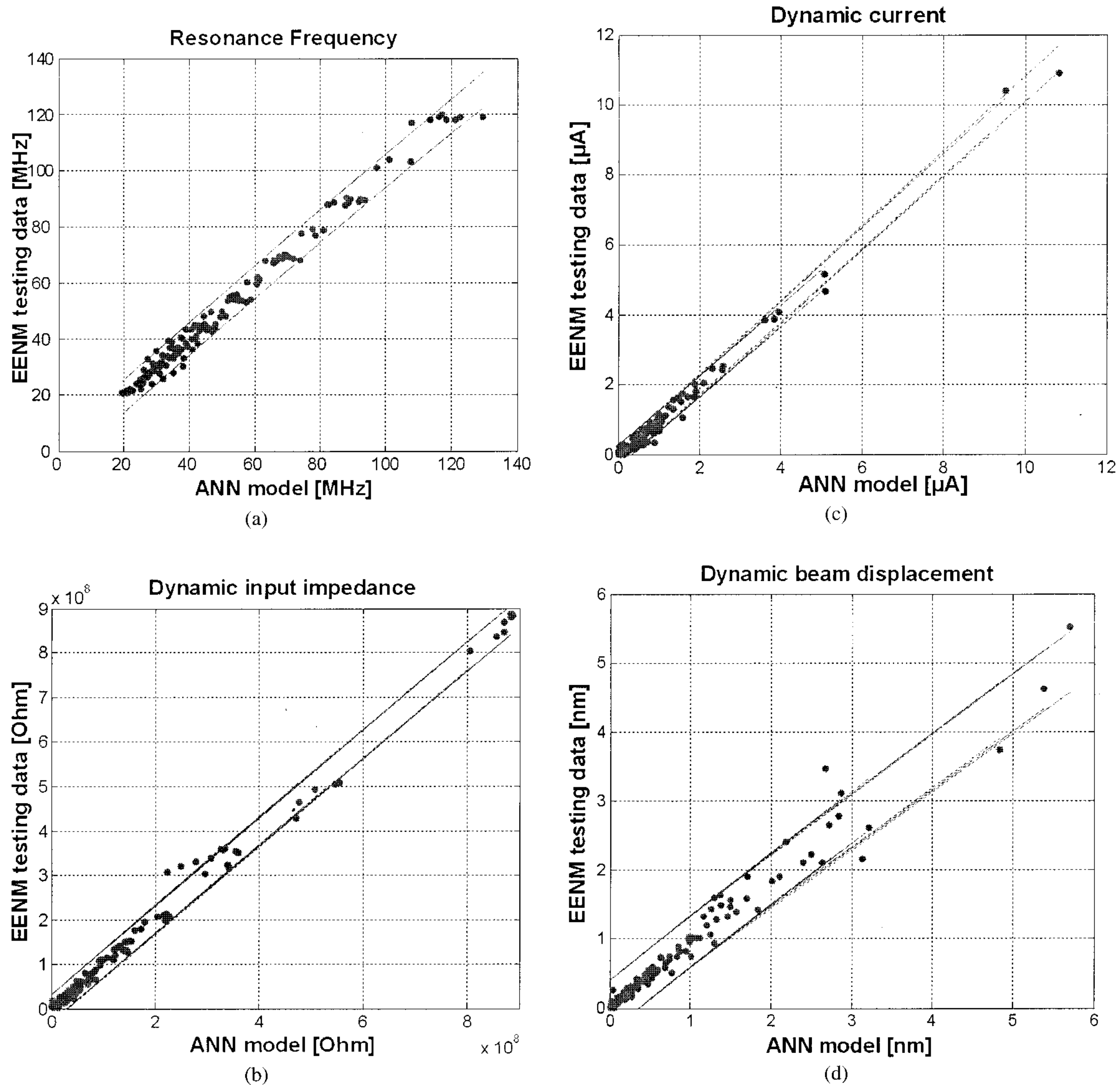

Figure 9. Comparison of the ANN-model results with the electrical-network model of the C-C beam resonator for the testing dataset: (a) resonant-frequency response with 0.9795 correlation coefficient; (b) dynamic-input impedance response with 0.9974 correlation coefficient; (c) magnitude of dynamic-current response with 0.9946 correlation coefficient; (d) magnitude of dynamic beam-displacement with 0.9818 correlation coefficient.

are applied, the vertical displacement of the resonating beam from the original position can be written as ($\bar{z}_i = z_i e^{j\varphi}$):

$$z(t) = z_0 + \mathrm{Re}\{\bar{z}_i e^{j\omega t}\} = z_0 + z_S(t) \qquad \text{(A4)}$$

By applying the Taylor-series expansion ($1/(1 \pm \Delta)^2 = 1 \mp 2\Delta + 3\Delta^2 \mp 4\Delta^3 + \ldots$ to eq. (A1), and for($|\Delta| \ll 1$ (as is the case here, ($\Delta = z(t)/d_0$)), we obtain the capacitance variation per unit displacement (note that the fringing fields are neglected at this time)

$$\frac{\partial C(t)}{\partial z(t)} \approx \frac{\varepsilon_0 A}{d_0^2}\left(1 + 2\,\frac{z(t)}{d_0}\right). \qquad \text{(A5)}$$

Due to the linearity of this configuration, we can superimpose these voltages and thus effectively state that the sum of the voltages is applied across the resonator's gap. The time-varying force is equal to the

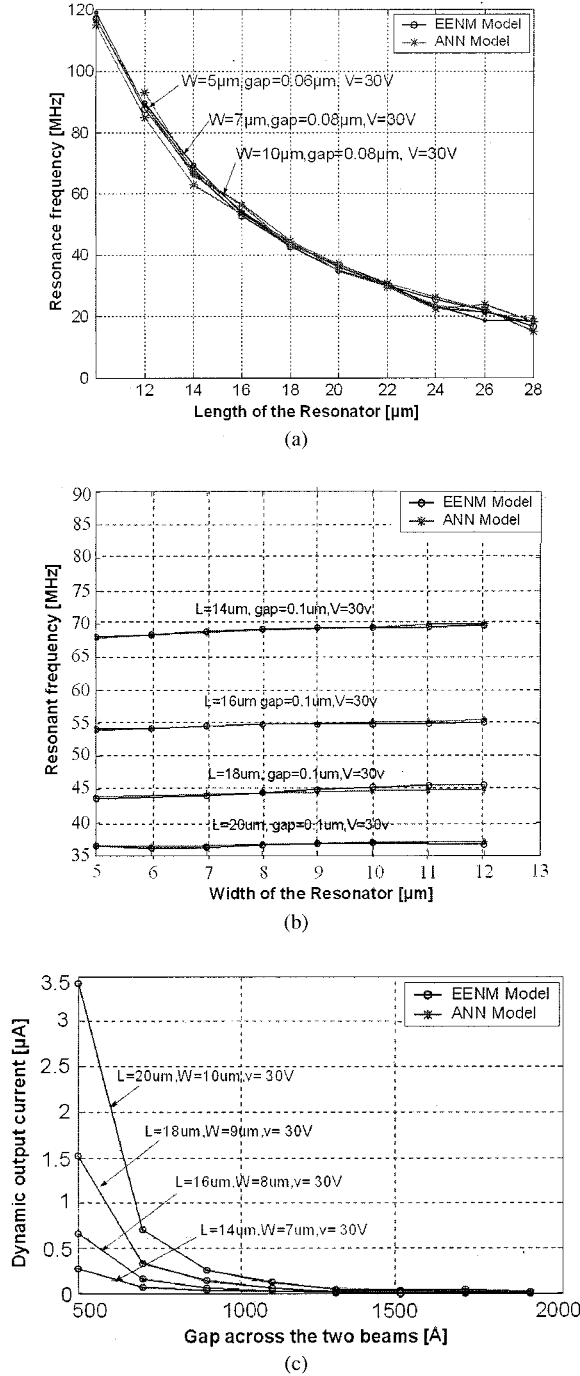

Figure 10. Various electrical responses from the trained ANN model with the change of geometrical parameters: (a) resonant frequency vs. resonating beam length; (b) static output current vs. resonating beam length; (c) resonating beam-to-electrode gap vs. dynamic output current.

rate of change of the stored electrostatic energy with time-varying displacement and is generated by the total voltages, while $v_i(t)$ and DC-bias voltage be-

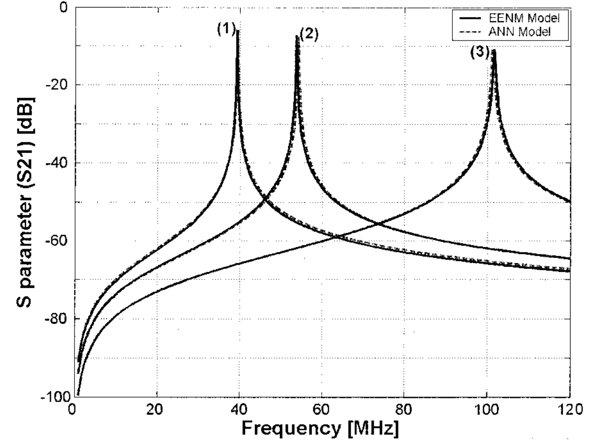

Figure 11. Comparison of the ANN model and EENM. Input parameters: (1) $L = 19$ μm, $W = 7$ μm, gap $= 0.08$ μm, and DC-bias voltage $= 30$ V; (2) $L = 16$ μm, $W = 7$ μm, gap $= 0.07$ μm, and DC-bias voltage $= 30$ V; and (3) $L = 11$ μm, $W = 8$ μm, gap $= 0.07$ μm, and DC-bias voltage $= 30$ V.

comes $\mathrm{Re}\{\bar{V}_i e^{j\omega t}\}$, (assuming $\varphi_{VI} = 0$) and V_p, respectively:

$$F(t) = \frac{\partial E}{\partial z(t)} = C_0 \cdot \left(\frac{V_P^2}{2d_0} + \frac{z(t)}{d_0^2} V_P^2 + \frac{V_P V_i e^{j\omega t}}{d_0} \right). \tag{A6}$$

We denote the terms in eq. (A6) as follows:

$$\bar{F} = F_0 + F_z + F_S,$$

where

$$F_0 = \frac{C_0 V_P^2}{2d_0},$$

$$F_z = \frac{C_0 V_P^2}{d_0^2} z(t),$$

and

$$F_S = \frac{C_0 V_P V_i e^{j\omega t}}{d_0}.$$

The first term, F_0 represents the electrostatic force that contributes to the deformation of the resonating beam. The second term, F_z is governed by the time-varying displacement of the resonating beam and the third term, F_s represents the time-varying force induced by the AC-excitation source. The total current through

TABLE IV. Comparison of Results from the ANN Model and EENM

	Resonant Frequency [MHz]			dB (S_{21})			Q Factor		
Model No.	1	2	3	1	2	3	1	2	3
ANN model	39.5	54.19	101.5	−5.33	−8.176	−9.935	975	709	377
EENM result	39.34	53.70	101.7	−5.350	−8.215	−9.987	968	713	376
Relative error	0.1%	0.074%	0.2%	0.037%	0.047%	0.052%	0.72%	0.56%	0.26%

the time-varying capacitor is composed of two terms as follows:

$$I_{Ci}(t) = \frac{\partial}{\partial t}(C(t)V_{Ci}(t)), \tag{A7}$$

$$I_{Ci}(t) \approx \frac{1}{1 + j\omega R_L C_0}\left(j\omega \frac{C_0}{d_0} V_P z_S(t) + j\omega \frac{C_0}{d_0} V_i z(t) + j\omega \bar{V}_i C_0\right), \tag{A8}$$

where $V_{Ci}(t) = (V_P + v_i(t))1/(1 + j\omega R_L C_0)$ is the voltage across the time-varying capacitance, and $z_S(t) = \text{Re}\{\bar{z}_i e^{j\omega t}\}$.

The second term in eq. (A8) can be ignored, since $v_i \ll v_p$ and it is very small compared to the first term; thus,

$$\bar{I}_{Ci} = \frac{1}{1 + j\omega R_L C_0}\left(j\omega \bar{V}_i C_0 + j\omega \frac{C_0 V_P}{d_0} \bar{z}_S\right), \tag{A9}$$

where the first term is the current through the capacitor C_0, and the second term is the current corresponding to the variations of the resonating beam $z_s(t)$. As seen in eq. (A9), the second term includes both electrical and mechanical parameters; thus, for a complete electrical-domain representation, the displacement $\bar{z}_S$ must be replaced with an electrical parameter. As shown in Figure 13(b), the mechanical motion of the resonating beam can be represented by an appropriate RLC parallel circuit. Finally, the currents through the resistor and capacitor can be expressed in terms of the inductor current i_L as

$$I_F = V \cdot \left(j\omega C + \frac{1}{R} + \frac{1}{j\omega L}\right),$$

where

$$\begin{aligned} V &= L\frac{di_L}{dt} \quad \text{and} \quad \frac{d}{dt} \to j\omega \\ &= i_C + i_R + i_L \end{aligned} \tag{A10}$$

Using electromechanical analogies, we obtain

$$V(t) \Leftrightarrow j\omega L z(t), \quad I_F(t) \Leftrightarrow LF(t)$$

$$\bar{z} = \frac{\bar{F}}{(j\omega C_D + K - \omega^2 M)},$$

where

$$\bar{F} = C_0 \cdot \left(\frac{V_P^2}{2d_0} + \frac{\bar{z}}{d_0^2} V_P^2 + \frac{V_P \bar{V}_i}{d_0}\right).$$

Therefore,

$$\begin{aligned} \bar{z} &= \frac{C_0}{(j\omega C_D + K - K_E - \omega^2 M)} \cdot \left(\frac{V_P^2}{2d_0} + \frac{V_P \bar{V}_i}{d_0}\right) \\ &= z_0 + \bar{z}_S, \end{aligned} \tag{A11}$$

electrical stiffness [N/m] is given by

$$K_E = \frac{C_0}{d_0^2} V_P^2.$$

As expected, $\bar{z}$ is composed of two terms: one is the electrostatic term, which is the off-resonant term when $\omega = 0$, and the other is the time-varying term. As indicated in eq. (A11), K_E is seen to be a function of the DC-bias voltage V_p and electrode-to-resonator gap d_0, which means that resonant frequency is tunable with the adjustment of the DC-bias voltage and electrode-to-resonator gap.

When the electrical stiffness is increased, the resonant frequency is lowered accordingly. From eqs. (A9) and (A11), the total current $\bar{I}_{Ci}$ exited on the resonator due to applied DC bias and AC excitation is given by

$$\bar{I}_{Ci} = \frac{1}{1 + j\omega R_L C_0}\left(j\omega \bar{V}_i C_0 + j\omega \frac{C_0^2 V_P^2 \bar{V}_i}{d_0^2} \frac{1}{(j\omega C_D + K - K_E - \omega^2 M)}\right). \tag{A12}$$

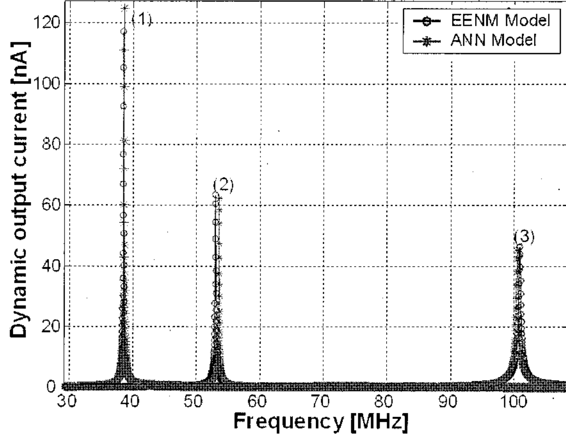

(a)

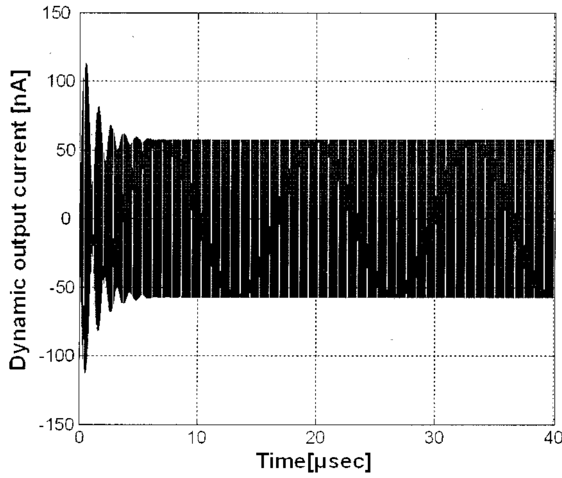

(b)

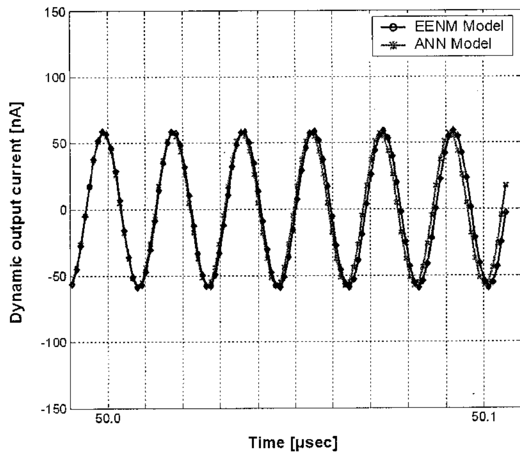

(c)

TABLE V. Corresponding Mechanical/Electrical Analogs

Mechanical Parameter	Units	Electrical Parameter	Units
Damping coefficient C_D	N/(m/s)	Conductance $G\ (= 1/R)$	Ω^{-1}
Stiffness $1/K$	$(\mathrm{N/m})^{-1}$	Inductance L	H
Mass M	Kg	Capacitance C	F
Force F	N	Current $(1/L)I_F$	A
Displacement z	m	Current $i_L\ (V/j\omega L)$	A

Assuming the denominator of the right-hand side of eq. (A12), $1 + j\omega R_L C0 \approx 1$, since $\omega R_L C0 \ll 1$:

$$\bar{I}_{Ci} = \left\{ j\omega \bar{V}_i C_0 + K_E C_0 \frac{1}{\left(C_D + \dfrac{K - K_E}{j\omega} + j\omega M \right)} \cdot \bar{V}_i \right\} = I_{C0} + I_{C1} \quad \text{(A13)}$$

As is seen, the current I_{c1} in eq. (A13) is dependent on the AC-signal source, $\bar{V}_i = V_i \cos\omega t$.

Finally, the input impedances seen at the excitation port of the resonator in the steady state [eq. (A14)] and in the dynamic state [eq. (A15)] are resepectively given by

$$Z_{\text{in_steady-state}} = \frac{1}{Y_{\text{in_steady-state}}} = \frac{1}{j\omega C_0}, \quad \text{(A14)}$$

TABLE VI. Comparison of Simulation Time for the Models

Model	Simulation Time
FEM model	70 sec
ANN model	1.37 sec
Implemented ANN model	1.49 sec

Figure 12. (a) Dynamic output-current comparison of ANN model with simulator result: (1) $L = 19\ \mu$m, $W = 7\ \mu$m, gap = 0.08 μm, and DC-bias voltage = 30 V; (2) $L = 16\ \mu$m, $W = 7\ \mu$m, gap = 0.08 μm, and DC-bias voltage = 30 V; and (3) $L = 11\ \mu$m, $W = 8\ \mu$m, gap = 0.07 μm, and DC-bias voltage = 30 V. (b) Dynamic output-current response in the time domain in the case of (2). (c) Larger view of Fig. 12(b): the response of the beam in the time domain between 50 μsec and 50.1 μsec. It is shown that good agreement is obtained between the ANN model and the simulator result.

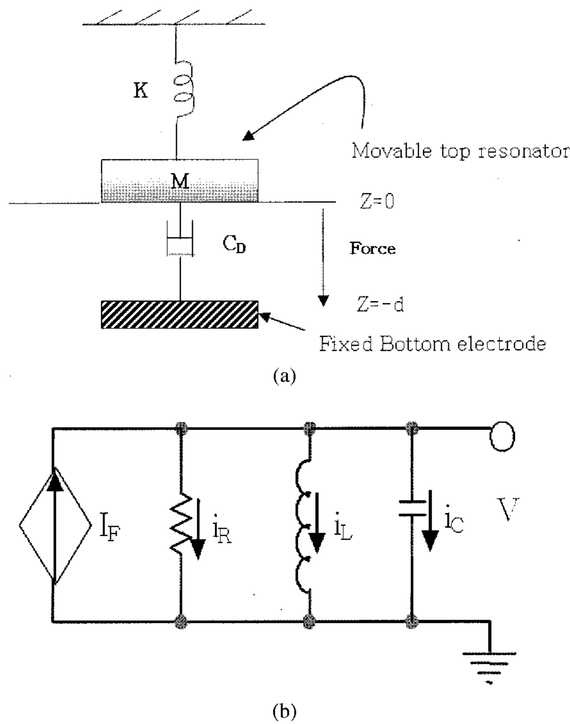

Figure 13. (a) Equivalent mechanical configuration for the C-C beam given in Fig. 1 and (b) equivalent parallel RLC circuit for Fig. 13(a).

$$Z_{\text{in_dynamic}} = \frac{1}{Y_{\text{in_dynamic}}} = \frac{1}{K_E C_0}\left(\frac{1}{R} + \frac{1}{j\omega L} + j\omega C\right). \tag{A15}$$

The time-varying capacitance is represented as the combination of static capacitance C_0 and a displacement-controlled current source (CCS). Voltage Controlled Current Source (VCCS) in the electrical analog is the dual of a voltage-controlled force in the mechanical system (see Fig. 14). Using the derived equations in section III, the electrical responses, as well as the physical responses from the C-C beam RF MEMS resonator, are obtained and compared with the results from the ANN model.

REFERENCES

1. J.Y. Qian, G.P. Li, and F. De Flavis, A parametric model of low-loss RF MEMS capacitive switches, Asia-Pacific Microwave Conf, Taipei, Taiwan 2001.
2. J.Y. Qian, G.P. Li, and F. De Flavis, A parametric model of MEMS capacitive switch operating at microwave frequencies, IEEE MTT-S Int Microwave Symp 2, 2000.
3. R.H. Krondorfer and T.C. Lommasson, Direct calculation of sensor performance in a FEA model [MEMS] Sensors, Proc IEEE 2 (2002).
4. N. Bushyager, K. Lange, M. Tentzeris, and J. Papapolymerou, Modeling and optimization of RF reconfigurable tuners with computationally efficient time-domain techniques, IEEE MTT-S Int Microwave Symp 2 (2002).
5. E.K. Chan, K. Garikipati, and R.W. Dutton, Comprehensive static characterization of vertical electrostatically actuated polysilicon beams, IEEE Design and Test of Computers 16 (1999), 58–65.
6. L. Rufer, C. Domingues, and S. Mir, Behavioral modeling and simulation of a MEMS-based ultrasonic pulse-echo system, Proc SPIE, Cannes, France, 2002, pp 171–190.
7. X. Lafontan, C.L. Touze, B. Wenk, I. Kolesnik, F. Pressecq, F. Perez, J. Nicot, M. Dardalhon, and S. Rigo. Environmental test bench for reliability studies: Influence of the temperature on RF switches with metallic membranes, Proc SPIE, 4755, pp 624–633, Cannes, France, 2002.
8. F.D. Bannon III, J.R. Clark, and C.T.-C. Nguyen, High-Q microelectromechanical filters, IEEE J Solid-State Circ 35 (2000).

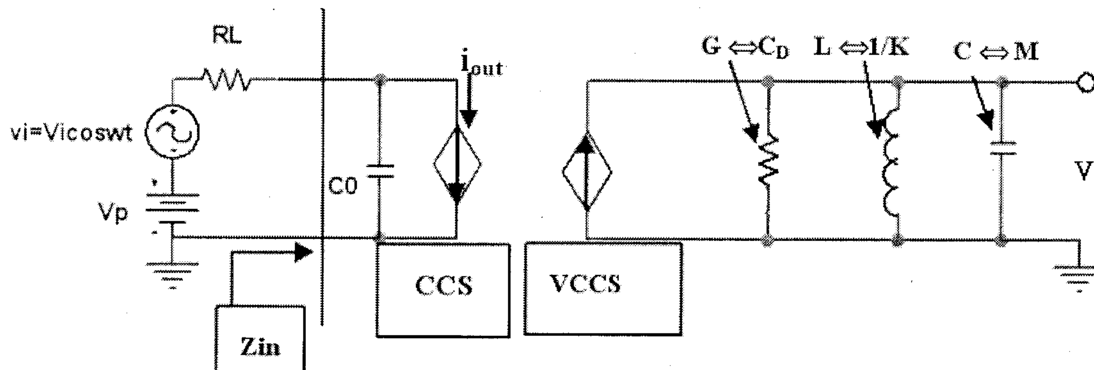

Figure 14. Electrical equivalent network model composed of the electromechanical force and the mass-spring mechanical system.

9. Y.H. Park and K.C. Park, Design sensitivity analysis for the performance evaluation of High-Q MEMS resonator, American Institute of Aeronautics and Astronautics, paper AIAA2002-1351, 2002.
10. MATLAB, R13, vers. 6.5, http://www.mathworks.com.
11. J.B. Muldavin and G.M. Rebeiz, High-isolation CPW MEMS switches, Pt 1: Modeling, IEEE Trans Microwave Theory Tech 48 (2000).
12. J.B. Muldavin and G.M. Rebeiz, High-isolation CPW MEMS switches, Pt 2: Design, IEEE Trans Microwave Theory Tech 48 (2000).
13. K.Wang, Y.Yu, A.C.Wong, and C. T-C. Nguyen, VHF free-free beam high-*Q* micromechanical resonators, 12th Int IEEE Microelectromechanical Syst Conf, Orlando, FL, 1999, pp. 453–458,
14. J.R. Clark, W.T. Hsu, and C. T.-C. Nguyen, Measurement techniques for capacitively transduced VHF-to-UHF micromechanical resonators, Int Conf Solid-State Sensors Actuators, Munich, Germany, 2001, pp.1118–1121.
15. C.T-C. Nguyen, Transceiver front-end architectures using vibrating micromechanical signal processors, Top Mtg Silicon Monolithic ICs in RF System, Ann Arbor, MI, 2001.
16. H.A.C Tilmans, Equivalent circuit representation of electromechanical transducers: II Distributed-parameter systems, J Micromech 7, (1997), 285–309.
17. T. Veijola, T. Mattila, O. Jaakkola, J. Kiihanmaki, T. Lamminmaki, A.O. Ja, K. Ruokonen, H. Seppa, P. Seppala, and I. Tittonen. Large displacement modeling and simulation of micromechanical electrostatistically driven resonators using the harmonic balance methods, IMS 2000, Boston, MA, 2000, pp. 99–102.
18. M.T. Hagan, H.B. Demuth, and M.H. Beale, Neural network design, PWS Publishing Company, Boston, 1996.
19. C.T.-C. Nguyen, Micromechanical circuits for communication transceivers, Proc BCTM, Minneapolis, Minnesota, 2000, pp.142–149,
20. M.T. Hagan and M. Menhaj, Training feed-forward networks with the Marquardt algorithm, IEEE Trans Neural Networks 5 (1994).
21. Advanced Design System, http://www.agilent.com.

BIOGRAPHIES

Yong Jae Lee was born in Seoul, Korea. He received his B.S. degree in electrical engineering from SungKyunKwan University, Seoul, in 1998. Currently he is working toward his Ph.D. degree in electrical and computer engineering at the University of Colorado at Boulder. His research interests include neural network modeling for RF MEMS devices and CAD of microwave devices and circuits.

Yong-Hwa Park received B.S. (1991), M.S. (1993), and Ph.D. (1999) degrees in mechanical engineering from the Korea Advanced Institute of Science and Technology (KAIST). In 1998, he was selected as a future frontier scientist by the Korea Research Foundation. During 1999, he joined the Acoustics and Vibration Lab. in the Korea Research Institute of Standard and Science (KRISS) as a Research Associate. At KRISS he worked on the standardization of human vibration characteristics. In 2000, he joined the MEMS research group in University of Colorado at Boulder (CAMPmode) as a research associate. From 2003, he has been working for the Visual Display Division, Digital Multimedia Network in Samsung Electronics Co., Ltd. in Suwon, Korea. His major research activity in MEMS area includes coupled-physics dynamic simulation of RF MEMS resonators, switches, and optical MEMS. His current activity in Samsung is development of big-screen projection display devices utilizing optical MEMS array. He is a member of the Society for Automotive Engineers and Society of Experimental Mechanics, KSME, KSNVE, and ASK.

Feng Niu is a Distinguished Member of the Technical Staff with Motorola Labs, Plantation, FL. He holds a B.S. in physics from Zhongshan (Sun-Yat Sen) University in China, and M.S. and Ph.D. degrees in electrical engineering from the Polytechnic University, Brooklyn, NY. He began his career with the Institute of Electronics, Chinese Academy of Sciences (CAS), Beijing, in 1983, and before joining Motorola in 1995, he was a research scientist with the Center for Advanced Technologies in Telecommunications (CATT), Brooklyn, NY. He has authored or co-authored 14 papers in peer-reviewed professional journals and proceedings. He has five issued US patents and eight more patents pending. He has been a technical reviewer for the IEEE journals in the areas of antennas, propagation, and communications. He has served on the international program committees and technical committees, and as session chairs and reviewers of the international conferences in the areas of systems, communications, antennas, and RF technologies. He has given invited technical presentations and keynote speeches for conferences, universities, and professional societies. He has more than 20 years experience as a researcher, engineer, and technical leader and his professional interests span such diverse areas as antennas, distributed sensing, data mining, location technology, MEMS, RF design, wave propagation, and wireless networking, as well as technology commercialization.

Bonnie Bachman is Director of Emerging Technology, iDEN Subscriber Group, Motorola, Inc., Plantation, FL. She holds a B.S. in physics from Benedictine University, Lisle, IL, an M.S. in materials science and mechanics from Rutgers University, New Brunswick, NJ, and a Ph.D. in materials science and engineering, also from Rutgers University. She was a Member of Technical Staff, AT&T Bell Laboratories before joining Motorola in 1998. She has authored or co-authored 34 papers in peer-reviewed professional journals and proceedings. She has four issued US, European, and World patents. She has served on 16 international technical program committees. Currently, she is chair of the Industrial Advisory Board for the NSF IURUC CAMPmode. She has given more than 50 invited technical presentations and keynote speeches for conferences, universities, and professional societies. She has served as an officer for several technical professional societies. She has more than 25 years experience as a researcher, technical leader, and manager. Her professional interests span such diverse areas as materials physics, electronic packaging, biosensors, location technology, MEMS, and pervasive computing. She is a Motorola representative to the Industrial Research Institute.

K. C. Gupta received the B.Sc. degree (Physics, Math and Chemistry) from Punjab University (India) in 1958, B.E. and M.E. degrees in Electrical Communication Engineering from the Indian Institute of Science, Bangalore, India, in 1961 and 1962, respectively, and the Ph.D. degree from the Birla Institute of Technology and Science, Pilani, India, in 1969. Dr. Gupta has been a Professor at the University of Colorado since 1983. Presently, he is also the Associate Director for the NSF I/UCR Center for Advanced Manufacturing and Packaging of Microwave, Optical and Digital Electronics (CAMPmode) at the University of Colorado, and a Guest Researcher with RF Technology Group of National Institute of Standards and Technology (NIST) at Boulder. From 1969 to 1984, he was a Professor in Electrical Engineering at the Indian Institute of Technology, Kanpur. From 1971 to 1979, he was the Coordinator for the Phased Array Radar Group of the Advanced Center for Electronics Systems at the Indian Institute of Technology. On leave from IITK, he has been a Visiting Professor at the University of Waterloo, Canada; at the Ecole Polytechnique Federale de Lausanne, Switzerland; at the Technical University of Denmark (Lyngby); at the Eidgenossische Technische Hochschule, Zurich; and at the University of Kansas, Lawrence. On sabbatical from the University of Colorado in 1993–93, Dr. Gupta was a Visiting Professor at the Indian Institute of Science in Bangalore and a Consultant at the Indian Telephone Industries.

Dr. Gupta's current research interests are in the area of computer-aided design techniques (including ANN applications) for microwave and millimeter-wave integrated circuits, nonlinear characterization and modeling, RF MEMS, and reconfigurable antennas. He is the author or co-author of eight books: *Microwave Integrated Circuits*) (Wiley Eastern, 1974; Halsted Press of John Wiley & Sons, 1974); *Microstrip Line and Slotlines* (Artech House, 1979; revised second edition, 1996); *Microwaves* (Wiley Eastern, 1979; Halsted Press of John of Wiley & Sons, 1980; Editorial Limusa Mexico, 1983); *CAD of Microwave Circuits* (Artech House, 1981; Chinese Scientific Press, 1986; Radio I Syvaz, 1987); *Microstrip Antenna Design* (Artech House, 1988); *Analysis and Design of Planar Microwave Components* (IEEE Press, 1994); *Analysis and Design of Integrated Circuit-Antenna Modules* (John Wiley & Sons, 1999); and *Neural Networks for RF and Microwave Design* (Artech House, 2000). In addition, he has contributed chapters to the *Handbook of Microstrip Antennas* (Peter Peregrinus, 1989); the *Handbook of Microwave and Optical Components, vol. I* (John Wiley & Sons, 1989); *Microwave Solid State Circuit Design* (John Wiley & Sons, 1988, 2nd edition, 2003); *Numerical Techniques for Microwave and Millimeter Wave Passive Structures* (John Wiley & Sons, 1989); and *Encyclopedia of Electrical and Electronics Engineering* (John Wiley & Sons, 1999). Dr. Gupta has published over 230 research papers and holds four patents in the microwave area.

Dr. Gupta is a Fellow of the IEEE (Institute of Electrical and Electronics Engineers, USA); a Fellow of the Institution of Electronics and Telecommunication Engineers (India); a Member of URSI (Commission D, USA); and a Member of the Electromagnetics Academy (MIT, USA). He is a recipient of IEE Third Millennium Medal and IEEE MTT-S Distinguished Educator Award. He is a member of the ADCOM for the MTT Society of IEEE, chair of the IEE MTT-S standing committee of Education, past co-chair of the IEEE MITT-S Technical Committee on CAD (MTT-1), a member of the IEEE Technical Committee on Microwave Field Theory (MTT-15), and earlier member of IEEE-EAB Committee on Continuing Education, and of IEEE-EAB Societies Education Committee. He is the founding editor of the *International Journal of RF and Microwave Computer-Aided Engineering,* published by John Wiley & Sons since 1991. He is an Associate Editor for *IEEE Microwave Magazine;* on the editorial boards of *IEEE Transactions on Microwave Theory and Techniques; Microwave and Optical Technology Letters* (John Wiley & Sons); and *International Journal of Numerical Modeling* (John Wiley & Sons, U.K.). He is listed in Who's Who in America, Who's Who in the World, Who's Who in Engineering, and Who's Who in American Education.

Dejan S. Filipovic received his Dipl. Eng. degree in electrical engineering from the University of Nis, Nis, Serbia and Montenegro, in 1994, and M.S.E.E. and Ph.D. degrees from the University of Michigan, Ann Arbor, MI, in 1999 and 2002, respectively. From 1994 to 1997, he was a Research Assistant at the School of Electrical Engineering, University of Nis. From 1997 to 2002, he was a Graduate Student Research Assistant at the University of Michigan. Currently, he is an Assistant Professor at the University of Colorado, Boulder. His research interests include antenna theory and design, as well as computational and applied electromagnetics. He received the prestigious Nikola Tesla Award for his outstanding graduate thesis, and won first place in the student paper competition at the IEEE AP/URSI Symposium held in San Antonio, TX.